H effects in Al-Mg, Al-Zn-Mg alloys and in Al: experiments, continuum and atomistic modeling

Döme Tanguy

H effects in Al-Mg, Al-Zn-Mg alloys and in Al: experiments, continuum and atomistic modeling.

D. Tanguy

dome.tanguy@univ-lyon1.fr

Institut Lumière Matière, UMR5306 Université Lyon 1-CNRS, Université de Lyon 69622 Villeurbanne Cedex, France

Abstract

Stress corrosion cracking of pure Al5%Mg is studied. It is shown by slow strain rate tests, constant force and cyclic traction-traction tests in a simulated confined medium that α ligaments (precipitate free) can be embrittled by hydrogen. Surface crack initiation in aged, annealed, 5083, after reversible H pre-charging, is modeled by a combination of digital image correlation and polycrystalline aggregate finite element simulation. It is shown, at the scale of the grain, that cracking occurs by a “decohesion” in between hard grains embedded in a deformation band. Cohesive zone modeling is used to quantify the possible impact of H weakened β precipitates on the global cohesion of a grain facet. It is shown that α embrittlement dominates. Finally, some basic aspects of hydrogen interactions with defects in Al are discussed, from atomic scale simulations: the stability of vacancy-hydrogen clusters, their mobility, hydrogen trapping, intergranular H and vacancy segregation and their impact on cohesion.

Keywords:

aluminum alloys, hydrogen embrittlement, grain boundary cohesion

Introduction

Aluminum magnesium alloys present an excellent resistance to corrosion that enables their use for light weight marine applications. Below 7%Mg (which is higher than the solubility limit at room temperature, about 2%), Mg remains in solid solution, called α, which provides hardening to the matrix {Osamura}. Optimal mechanical properties are reached by an additional cold work (rolling). During the extended lifetime of structures, the solid solution decomposes with a rate that is function of temperature (see other papers in this volume), preferentially in the vicinity of grain boundaries, producing discontinuous Mg-rich precipitates called β.

Although less studied than high strength aluminum alloys {Holroyd2011, Holroyd2013, Gangloff, Scully2012}, substantial efforts have been devoted to the study of the impact of such aging on the susceptibility to Stress Corrosion Cracking (SCC). Reviews are presented in other papers in this volume. In brief, there seems to have a consensus saying that {Jones2003}, ``fast" crack propagation (between 1 and 100 nm/s) stems from sequences of anodic dissolution of β precipitates, producing hydrogen (H), which diffuses ahead of the crack tip and embrittles the ligament in between the precipitates. More specifically, we can mention a few recent contributions addressing: the characterization of β precipitation {Goswami}, the effective H diffusion coefficient in the matrix, including the influence of concentration {Scully2013} and the boost of crack propagation

velocities (up to 10^4 nm/s) due to prolonged aging {Crane2012}.

In this paper we want to present an enriched synthesis of our previous work where we tried to contribute to the understanding of hydrogen effects during grain boundary (GB) fracture: First on β-free, pure, Al5%Mg and later on commercial AA5083 with a moderate aging. We tried to complement experiments (essentially fracture tests) with calculations at different length scales which addressed the following issues: The role of local stresses versus local strains on surface crack initiation after, reversible, H charging; the impact of a sequence β precipitate / α ligament on GB cohesion, when β is supposed to be weak with respect to the ligament. At that point the paper deviates from SCC of Al5%Mg and deals with H embrittlement, in general. First, we present internal hydrogen embrittlement fracture tests and their modeling based on cohesive zones coupled to hydrogen diffusion. The reader is warned that this section concerns AlZnMg alloys. Second, the interaction of hydrogen with vacancies, in particular the mobility of the clusters, is modeled, following our extensive work on the Ni-H system, from the ab initio data in the literature. Finally, H and vacancy segregation to grain boundaries, in Al, and their implication on cohesion are discussed.

The different parts of the paper follow this order, starting with a brief description of the materials, H charging and mechanical testing procedures. Finally, we will present some perspectives.

Materials, hydrogen uptake and cracking

Mechanical tests were conducted on two materials: pure Al5%Mg {Tanguy2002} and AA-5083 {Pouillier}. Both materials had equiaxed grains with no texture and grain sizes of 100 µm and 25 µm respectively. There was already convincing evidence, in the literature, that Al-Mg alloys can be H embrittled when β precipitates are present at the grain boundaries {Ohnishi1980, Malis1982, Holroyd1985} and, therefore, we chose to work first on a pure, β free, microstructure. The control on solute concentration was focused on Fe and Si to decrease the concentration of nano-scale dispersoids, in comparison to industrial 5083. The composition was 5.05% Mg, 0.04% Fe and 0.04% Si, in weight. Concentration in other elements was not decreased in comparison to 5083. The samples were solution treated after a natural aging of 16 years. No β precipitation was visible in TEM (although some precipitation remained at the triple points).

A series of mechanical tests were considered: slow strain rate tests (SSRT), constant force (Static) and cyclic force tests (FC, for fatigue corrosion). Two environments were used: NaCl 30g/l + HCl (pH=4.3) and $AlCl_3$ 120g/l (pH=2.4, de-aerated by nitrogen bubbling). The later was supposed to represent a confined solution, such as the one found in deep single cracks. The goal was to show that we could produce, fast, single cracking, in the absence of β phases, and that the main driving force was H, if its uptake was stimulated.

First SSRT on smooth samples, in NaCl, showed a very strong resistance to SCC: although the GBs were attacked, only short multiple cracks were obtained after 30 days of SSRT at $\dot{\epsilon}=10^{-7}\,s^{-1}$ (30% elongation was reached without failure). It was only when samples were pre-strained that a long crack could emerge from the population of short cracks. Therefore, we systematically applied 30% pre-straining, at high velocity (10^{-3} s^{-1}). The specimen were initially annealed with a yield strength as low as 60 MPa (elongation to fracture about 50%). The yield strength went up to 230 MPa. In addition, a thin notch (100 µm thick and about 300 µm long) was machined on one side of squared section (4×4 mm², gage length 12 mm) of the samples (Fig. 1a). This favored solution confinement, and established reproducible, fast, single cracking. Table 1 gives the order of magnitude of the average propagation velocity, in NaCl 30g/l at free corrosion potential: 7 nm s^{-1}. This velocity is simply the ratio of the depth reached by the IG crack, measured post mortem on the

fracture surface, by the duration of the test. To evaluate the reliability of this estimate, since no crack length monitoring was used and that the total test duration contains the initiation time (time to form an IG crack and solution confinement) and the final ductile fracture time, consider that one test was interrupted after 2 days of SSRT and that the crack had already propagated by 1 mm, which gives a velocity of 5.8 nm s^{-1}. Another test fractured after 5.7 days and gave an IG depth of 4.2 mm (8.5 nm s^{-1}). This crack velocity is well in the range reported in {Crane2012}, in NaCl at -800 mV/SCE and low DOS level: from 1 to 10 nm s^{-1}, in view of the variability due to the applied K. It is significantly faster than the one reported in {Jones2001} (0.1 nm s^{-1}) which are close to the slow propagation we observed when the samples were not pre-strained at high velocity (we observed 0.23 nm s^{-1}). Note that, in this case, initiation might have been long due to multiple cracking on the smooth samples.

Second, a simulated confined environment was used $AlCl_3$ 120g/l (all samples have a similar notch as above). The oxygen was removed to reproduce occluded cell conditions and stimulate H production. All tests were performed are free corroding potential, of the order of -840 mV/SCE. A slow general dissolution of the sample was observed. It reproduced the order of magnitude of the crack propagation velocity obtained in natural confinement {Tanguy2002}: 3.8 nm s^{-1} (Table 1). In Table 1, the comparison between the different loading modes, in $AlCl_3$, suggests an important role played by plastic deformation during IG cracking, in preference to a role of the macroscopic stress. Indeed, when comparing SSRT and static force tests, the crack propagation is drastically diminished as strain rates goes down, while the average stress remains high enough (170 MPa) to observe IG fracture when the load is cyclic (Table 1 and caption). These are traction-traction tests and the high R ratio limits the compression at the tip during the unloading part of the cycle. We therefore view them as dynamic traction strain tests at low average stress levels. What could be the role of this local plastic deformation, knowing that the samples are already heavily plastically deformed with consequences on GB sliding and hardening of the matrix around the tip? We propose a role on H production and entry, even though no traces of accelerated dissolution could be seen on the fracture surfaces.

Mechanical loading		Environment	E_{OCP} (mV/SCE)	$\dot{v}$ (nm s^{-1})	N_R
SSRT	$\dot{\varepsilon_0}=10^{-7}s^{-1}$	NaCl 30g/l + HCl (pH 4.3)	~-780	7	
SSRT	$\dot{\varepsilon_0}=10^{-7}s^{-1}$	$AlCl_3$ 120g/l (pH 2.4) deaerated	~-840	3.8	
Static	$\sigma_0=220$ MPa $\dot{\epsilon}=10^{-8}s^{-1}$	-	-	1.8	
Static	$\sigma_0=170$ MPa $\dot{\epsilon}=1.7\,10^{-9}s^{-1}$	-	-	-	
FC	$\sigma^0_{max}=190$ MPa	-	-	12.2 (9.1)	7800
FC	$\sigma^0_{max}=170$ MPa	-	-	13.1 (7.5)	9500
FC	$\sigma^0_{max}=150$ MPa	-	-	12.6 (6.2)	14000
FC	$\sigma^0_{max}=110$ MPa	-	-	5.7 (3.5)	37000
FC	$\sigma^0_{max}=60$ MPa	-	-	-	-

Table 1:

Averaged velocities $\acute{v}$ obtained by dividing the intergranular crack length by the duration of the fracture test, as a function of mechanical load, for Al5%Mg in two different environments{Tanguy2002}. All samples have similar notches (Fig. 1). SSRT means Slow Strain Rate Testing and is conducted at an initial strain $\acute{\varepsilon}_0$. FC (fatigue) is for a triangular cyclic load, at different initial maximum stress levels σ^0_{max} , constant force ratio $R=F_{min}/F_{max}=0.5$ and f=0.1 Hz. Velocities in parenthesis are initial velocities, assuming the instantaneous velocity is proportional to the stress level during propagation $v=\alpha(\sigma-\sigma_c)$ with σ_c=60 MPa a threshold stress and α=0.006 mm (MPa day)$^{-1}$. E_{OCP} is the electrochemical potential at open circuit and N_R the number of cycles at rupture.

Smooth intergranular fracture surfaces were produced (Fig. 1b and c). No traces of striations were observed, contrary to 7XXX alloys {Young2002, Holroyd2011, Holroyd2015}. However, even if the dimensions of the samples are much reduced in comparison to standardized fracture samples, the fracture surface remained several hours in contact with the solution and was therefore always slightly corroded. It prevented the search for fine scale features on the fracture surface, even if the deaeration drastically decreases the corrosion rate. This is partly the motivation for studying cracking, in air, due to internal H. An additional experiment was made: a sample was sliced parallel to the fracture surface, immediately after single cracking, and bent. It was observed that secondary cracks can be opened (even running parallel to the main crack) upon bending (Fig. 2). It indicates that the crack wake is brittle, but not beyond one grain.

Experiments were pushed further with the idea to simplify the processes, i.e. to try to separate the embrittlement effect from the complex H uptake conditions enhanced by active plasticity. It was first observed that pitting at triple points (15 days exposure to HCl solution at pH=1.5 and free potential) produces an embrittlement of adjacent grain facets {Tanguy2002}, as observed after traction at $\acute{\varepsilon}_0=10^{-5}s^{-1}$. This damage, additional to the dissolution of the triple point, was reversible after one week at room temperature. We believe H, produced by pitting, was involved {Tanguy2002}. The embrittlement was always very close to corroded triple points. Its depth was of the order of 10 µm. This is significantly smaller than the penetration depth (Λ) one would expect with a diffusion coefficient of $D_{eff}=10^{-14}$ m²s^{-1} (first H uptake in permeation tests where dissolution of the surface is active, possibly involving coupled vacancy-H diffusion {Scully2013}), as evaluated by $\Lambda=\sqrt{D_{eff}t}$ with the time t equal to 15 days ($\Lambda\sim110$ µm). In addition, the embrittlement length did not increase with prolonged exposures to the pitting corrosion. It even disappeared, which may mean that H production was reduced at some point and H desorbed.

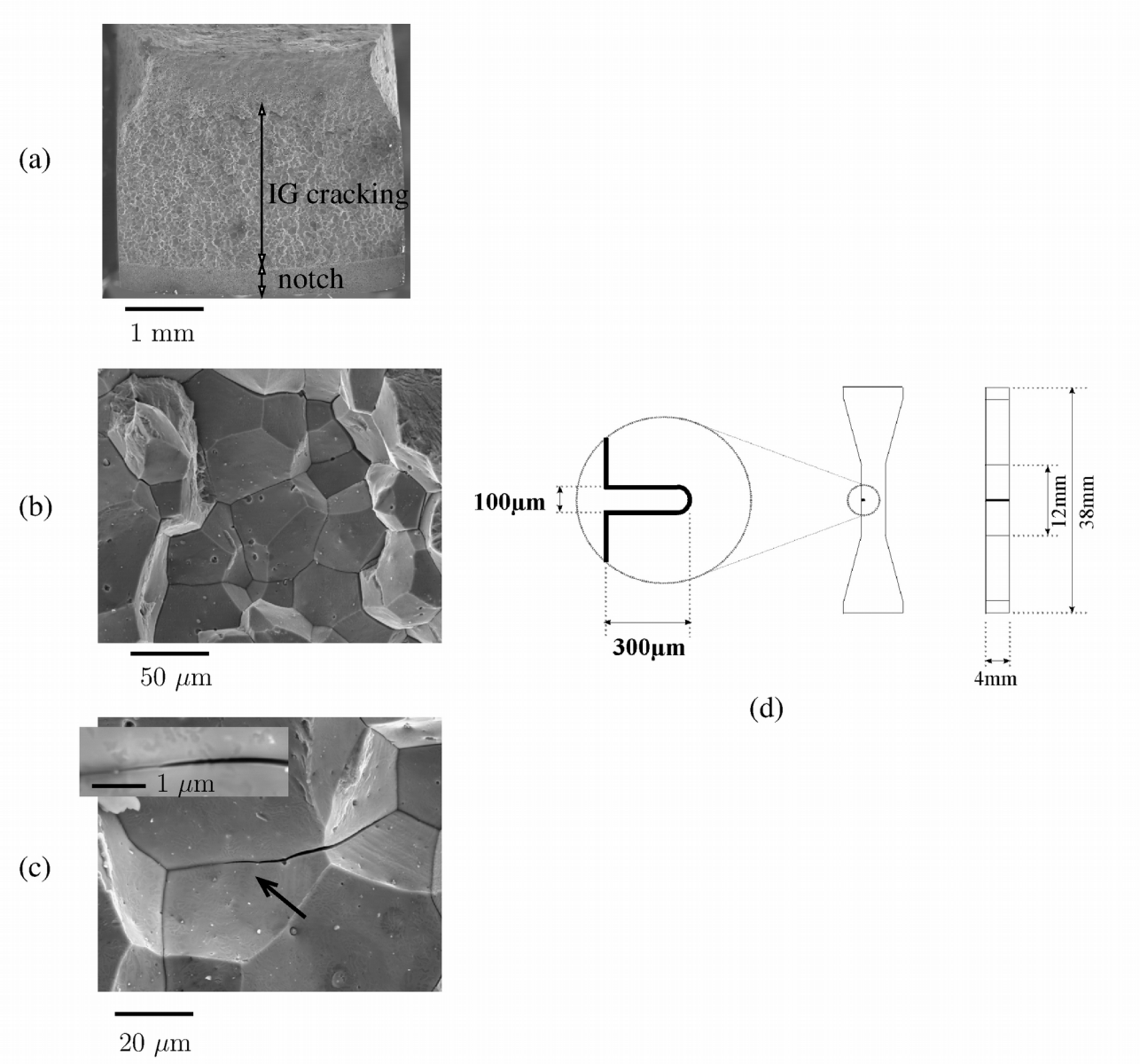

Figure 1:

(a) Fracture surface of a notched, β free, pure Al5%Mg, specimen after cyclic loading ($\sigma^0_{max}=110$ MPa, $R=F_{min}/F_{max}=0.5$, f=0.1 Hz) in $AlCl_3$, (b) typical intergranular fracture and (c) a zoom (insert) on a secondary crack tip (marked by the arrow). Grains are equiaxed with grain size of the order of 100 μm. (d) A schematic representation of the samples' geometry showing the notch's dimensions.

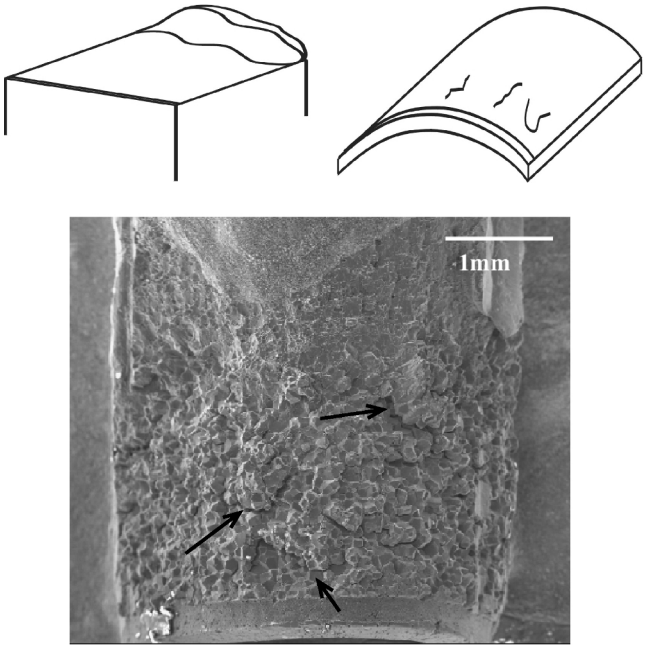

Figure 2:

The sample was sliced parallel to the fracture surface and bent. Intensive secondary cracks were opened (arrows), showing that the GBs were embrittled all along the crack wake, but no deeper than one grain size.

A second series of experiments was conducted with the goal to find more reliable conditions for H uptake and a damage that could be reversed upon heat treatment (i.e. H embrittlement with little or no surface damage). It is recalled that H uptake in Al alloys is not easy because of the energetics of adsorption and the properties of the oxide layer {Scully2012}. Motivated by the SSRT results in $AlCl_3$ (hydrated $AlCl_3$ 120g/l, pH=2.4, deaerated by nitrogen bubbling), this solution was selected for applying a moderate cathodic polarization (-1mA/cm²) for a time as long as possible. It was found that 12 hours was a good compromise. Serious surface damage occurs on longer exposure times. Exposed samples where deformed in traction (at high velocity). It was found that, in the absence of β along the GBs, no significant embrittlement was observed (max 1 µm depth), while samples submitted to the conventional heat treatment 7 days at 150 °C, were sensitized to H embrittlement. This heat treatment is supposed to be equivalent to 30 days at 100 °C (DoS 50 mg/cm^2 {Birbilis}) but the DoS was not characterized. Since GB embrittlement was obtained after triple point pitting (β dissolution) in otherwise β free microstructure, this result might mean that H uptake is not sufficient, under such cathodic polarization, to induce H fracture of the α ligaments. A similar result is reported in {Crane2012} for a pre-charging in NaOH where patches of brittle GBs where observed only in the presence of β precipitates (high DoS). We will show, in the modeling section below, that a direct role of embrittled β precipitates on the cohesion of the composite α/β GB is unlikely, i.e. the embrittlement of the α ligament dominates. Therefore, we think that β plays a role in the H entry in the material at cathodic polarization. This also tend to show that mechanical loading, in a medium that could generate enough H for embrittlement (Table 1), is necessary for generating enough H to induce fracture of the α ligaments, in the absence of β.

This heat treatment and H uptake procedure was then applied to AA-5083 {Pouillier}. A heat treatment of 1h at 400 °C removed any trace of embrittlement which definitively proved that H was responsible for fracture and that the electrochemical charging did not produce any significant GB oxidation on the surface (grooving) that could be mistaken for H embrittlement. The embrittlement depth was of the order of one grain size (25 µm), which agrees well with the penetration depth

$\Lambda \sim 20$ µm after 12 hours. However, we observed again that no additional embrittlement could be obtained if the charging time was pushed further.

As a conclusion of this section, SCC of pure, β free, Al5%Mg has been studied. It was shown, by SSRT with solution confinement in notches compared to SSRT in simulated confined medium and triple point pitting in acidic solution, that the α ligaments can be embrittled by H. The comparison of traction-traction cyclic tests, constant force tests (with decreasing creep rates) and SSRT tends to show that some dynamic plasticity, in preference to high macroscopic stress levels, was essential to obtain H damage. With the intention to further study the influence of H on GB cohesion, H was electrochemically pre-charged in the sample. The rest of the paper deviates from SCC and focuses on H damage, independently of H uptake. The next section is devoted to the mechanical modeling of H pre-charged samples fractured in air or in vacuum. The first case is a plastic polycrystalline aggregate model coupled to in situ monitoring of surface crack initiation in sensitized 5083 samples. Digital image correlation is used to measure strains and the model used to evaluate the corresponding local stresses. The second case is devoted to the effect of internal hydrogen on the cohesion of a composite GB modeled by cohesive zones. Finally, we present a set up for testing the effect of lattice hydrogen on GB fracture. The author is warned that the results concern an AlZnMg alloys and not an Al5Mg alloy. Nevertheless, the experiments and the modeling of H transport during crack propagation are relevant to H embrittlement in general, as we will show.

Mechanical modeling

Influence of local stresses versus local strain on H related cracking at the surface of AA5083

Commercial alloy 5083, as described above, was charged with hydrogen by a direct exposure to the $AlCl_3$ solution, with the suitable amount of β precipitation to observe, reversible, H damage of the grain boundaries at the surface. The goal is to follow the crack initiation at an intermediate scale (the scale of the grain) and determine the local conditions for GB fracture, i.e. determine, by a combination of deformation field measurements and simulation of local stresses, a criterion for initiation. First, on the experimental side, EBSD was used, prior to H charging, to map the grains on the surface and determine their orientation. Traction tests were performed in a SEM. The traction curve was recorded and pictures of the surface were periodically taken. Tiny oxides on the surface were used to perform image correlation and measure the deformation fields at various magnifications (Fig. 3). Crack initiation is detected by the discontinuities in the measured displacement fields.

On the simulation side, a crystal plasticity model for Al5%Mg is developed and reproduces the macroscopic traction curve (elastic limit and hardening). The real polycrystalline structure, such as determined by EBSD on the surface, is meshed. The experimental orientation of each grain is introduced in the model. The model is 2D, but the grains are extruded in the third dimension (generalized plain strain). The polycrystal is stretched in traction and the local deformations obtained are compared to the fields obtained by image correlation. The model is in good qualitative agreement with experiments, i.e. the zones of high and low deformation are well reproduced (Fig. 11 a, b and 12 of {Pouillier}). Then, the local tractions along the GB facets are extracted from the model and the local stresses in the zones where the cracks are observed experimentally are analyzed.

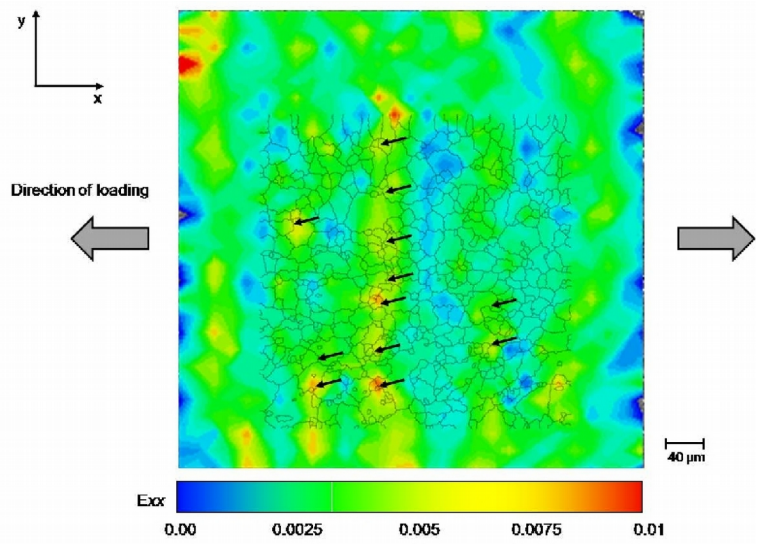

(a)

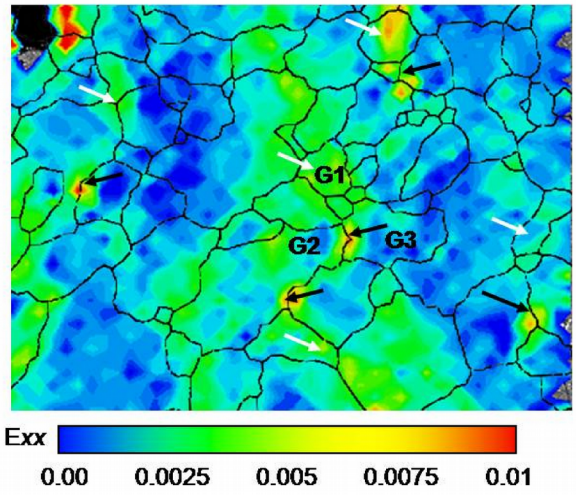

(b)

Figure 3:

Deformation field (Exx is the xx component of the deformation tensor), obtained by image correlation, during traction tests on AA-5083 with β intergranular precipitation, after H charging {Pouillier} by a direct exposure to an $AlCl_3$ solution. (a) and (b) are different magnifications. Black arrows point at cracks. White arrows point at areas of high deformation. Pictures reproduced, with modification, from {Pouillier}with permission from Elsevier.}

At low magnification, deformation appears localized in macroscopic bands perpendicular to the traction axis. Multiple crack initiations are detected in such bands (initiation occurs after the macroscopic yield point). At a medium magnification, it is observed that initiation occurs, within deformation bands, but always in between grains which deform less than their surroundings (these are called “hard” grains, but it does not mean that they have been hardened by plastic deformation or oriented in such a way that slip systems are not active, the low deformation also depends on how the neighbors deform and the shape of the grains), as illustrated by figure 5 where a crack appears between grains G2 and G3, at the point shown by the black arrow. It is therefore a brittle cracking occurring in between two “hard” grains in a polycrystalline environment where deformation is active. The crystal plasticity calculation gives an average stress on the GB facets at the moment of cracking of 175 MPa (variations are in the range 135 to 205 MPa, while the macroscopic yield strength is 85 MPa). The criterion proposed for crack initiation is therefore a critical local stress (an

average on a facet) for decohesion. The detailed argumentation which supports this criterion has to be read in the original paper {Pouillier}. The low stress level, in comparison to the yield point of work hardened 5083 alloys might be puzzling, although traction-traction tests (Table 1) have shown the stress can be decreased to levels between 60 and 110 MPa, which are lower than the threshold of 175 MPa. A possible reason is that the damage induced by the pre-charging procedure is stronger than the one the GBs undergo in SCC or maybe some stress concentration was involved at the surface during initiation (at triple points for example).

Effect of the density of brittle β precipitates on cohesion

The question we want to address is: what is the influence on toughness of the β-matrix interfaces, if they are even more brittle than the α ligaments? The idea that the precipitates preferentially trap H is motivated by the TEM observations of bubbles formed at the β-matrix interfaces, after exposure to hot water vapor {Malis1982}. Decohesion was also observed there. A nanoscale cohesive zone (CZ) is used to model, within continuum mechanics, the influence of, generic, brittle precipitates on cohesion, in the absence of plastic deformation (ideal work of fracture) {BenAli2013}. The CZ is a non linear traction / separation law $T_n(\Delta_n)$ which describes the mechanical properties of the fracture process zone (FPZ), immediately ahead of the crack tip, in the region where the elastic solution is not valid (we stress that it is a nanoscale FPZ and that the plastic zone is not considered). It has a generic shape which can be derived from the universal binding equation of Rose {Rose1981} and written {Needleman1994} as:

$$T_n(\Delta_n) = -\sigma_{max} \frac{\Delta_n}{\delta_c} e^{1-\Delta_n/\delta_c} \qquad (1)$$

The CZ is implemented in a two dimensional system containing a semi-infinite crack which is loaded mechanically in opening mode I by applying the elastic displacement field (applied stress intensity factor K_I) on a circular boundary far from the nonlinear process zone. An interface, which mechanical properties are given by Eq. 1, runs in front of the crack tip. Two sets of parameters have to be chosen: the ones representing the brittle α ligament and the one representing the H embrittled β precipitates. The procedure is empirical. First, the "ideal work of separation", which represents the area under the traction-displacement relation is fixed to a reasonable value (2.7 J/m^2) representative of metal single crystals and ceramics cleavage {Needleman1987, BenAli2013}. This value is transformed into the theoretical toughness (K_{Ic}), with Griffith's formula. An additional relation is required. It comes from the estimate of the FPZ length (L), obtained analytically in the case of a rectangular CZ model (Barenblatt): $L = \frac{9\pi}{32}\left(\frac{K_{Ic}}{\sigma_{max}}\right)^2$. It shows that, at fixed work of separation, the higher the maximum stress in the FPZ, the shorter the length of the FPZ. The parameters chosen for the H embrittled α ligaments (described by CZ_1) are $\sigma_{max} = 1$ GPa at a critical opening $\delta_c = 1$ nm. With these parameters, the critical stress intensity factor for the onset of crack propagation is K_{Ic}=0.46 MPa $\sqrt{m}$ and the typical dimension of the FPZ is 190 nm. This value is large enough to ensure that once the crack meets an α ligament, the FPZ extends enough to cover at least one β precipitate and therefore that there will be an interaction in between both FPZ.

A second CZ model (CZ_2) is defined where $\sigma_{max} = 0.25$ GPa. This is supposed to represent the weakened matrix-β interface. This choice is motivated by {VanDerVen} where it is suggested that H can decrease σ_{max} by a factor 5. Both choices emphasize the potential embrittlement effect of the β precipitates.

Then, model composite microstructures are constructed from CZ_1 and CZ_2 cohesive zone elements.

The sizes investigated are 50, 100, 150 and 200 nm for both precipitates and α ligaments. All combinations where tested. Then the applied load is raised until the onset of brittle propagation, which gives a numerical estimate of the toughness of the microstructure. The sequence precipitate / α ligament always starts with an α ligament in front of the crack (otherwise cracking would always occur when the weak precipitate toughness is reached and stop when meeting the first α ligament). If a ligament larger than 190 nm (the process zone size corresponding to a homogeneous grain boundary of characteristic CZ_1, i.e. completely free of β precipitates) is considered, for example 200 nm, then the crack will not feel the presence of the weak precipitates. Cleavage, with a very narrow process zone, should not be sensitive to the presence of weak points along GBs. On the contrary, small ligaments / large precipitates will give lower toughness, which is intuitive. The influence on toughness of both characteristic lengths is linear {BenAli2013} (note that in {BenAli2013}, the color box of the stress maps is incorrect, the stress values should be divided by a factor 2: they are normalized by the maximum stress and therefore lower than 1). The magnitude of the decrease is not intuitive: the combination of 50 nm long ligaments with 200 nm long precipitates gives a toughness 78% of the value of the precipitate free toughness. Furthermore, by construction of the model, this value can be considered as a lower bound (the 2D configuration also emphasizes the effect of the brittle β). This surprisingly high value suggests that it is the embrittlement of the α ligament which dominates the overall embrittlement. Note that the situation considered here is static: H doesn't desorb; it doesn't accumulate in the form of bubbles at broken β-matrix interfaces. Therefore, a potential benefit coming from the removal of H from the ligaments and storage in the broken precipitates, as proposed by Scamans {Scamans1976}, is not considered in the model.

Owing to the empirical choices of the σ_{max} values, the predictive capabilities are limited. However, if a true embrittlement of the GBs could be obtained (i.e. a traction rate independent brittle fracture), by internal H, the variation of the GB embrittlement with precipitate size and precipitate spacing such as characterized by Birbilis {Birbilis}, would give information about the length of the PZ of the brittle a ligament. In particular, no variation would suggest a PZ smaller than 100 nm, i.e. a high value of σ_{max} in the PZ.

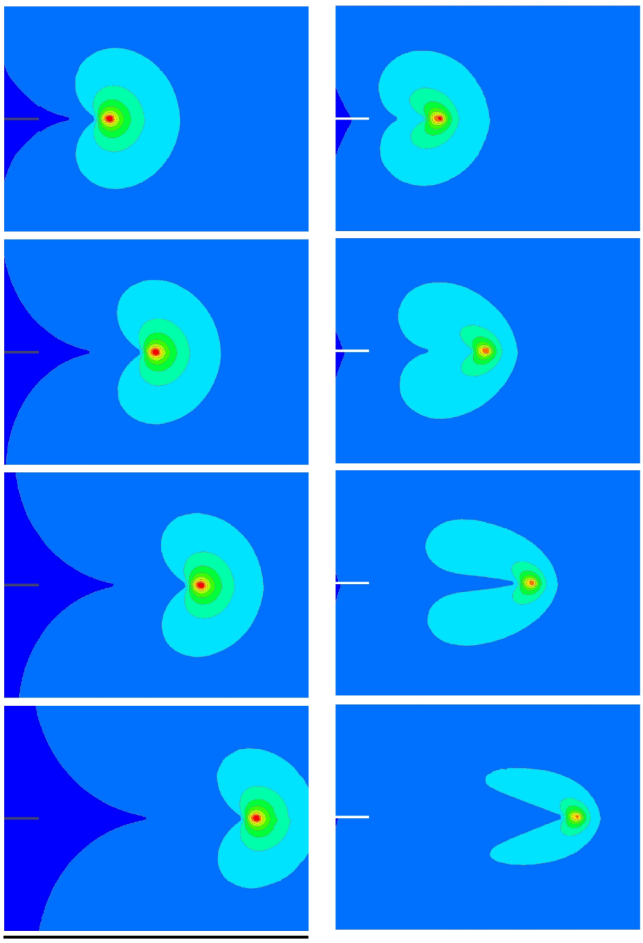

Figure 4:

Time evolution of the hydrogen distribution during crack propagation, starting from a homogeneous distribution, with $D_{eff}=10^{-12}$ m^2s^{-1} and crack propagation velocities of 1500 nm/s (left) and 7500 nm/s (right) {BenAli2012}.

Gruhl's experiment revisited and H diffusion as a rate limiting process in the case of internal hydrogen: H pre-charged AlZnMg alloys

At this point, we deviate from SCC of Al5%Mg and consider the mechanisms of H induced intergranular decohesion in the case where H is initially homogeneously distributed in the lattice (and at equilibrium with microstructural traps). The motivation is to gain insights on H-GBs interactions in a case which is simpler than SCC. Indeed, we have seen in the different cases above that H uptake, from an electrolyte, has complex connections with the microstructure: β dissolution at the crack tip creates an extreme acidic medium and an H overpotential that boost H production and entry (see the boost in crack propagation velocities in {Crane2012} in $AlCl_3$ + $MgCl_2$ at -1000 mV/SCE, with respect to the values in Table 1 in $AlCl_3$ pH=2.4), the presence of β at the surface during H cathodic charging involves a large difference in the subsequent damage, the pitting of triple points (β decorated) induced an embrittlement which low extension is not rationalized by H diffusion, not even with the slowest diffusion coefficient known. For all these reasons, we moved to an experimental set up which aims at introducing H in the sample independently of the electrochemical processes that would occur if directly immersed in the electrolyte.

We revisited the hollow tube test by Gruhl {Gruhl1984}. Thin, flat, traction specimen of section 2 mm^2 (2 mm wide / 1 mm thick) were prepared. A 30 µm thick, nano crystalline, Ni layer is

deposited. One face is exposed to an acid solution and H is electrochemically charged into the sample through the Ni layer. On the opposite face, a thin and short notch is machined (100 µm depth and 50 µm circular radius at the tip). The results concern an Al-Zn-Mg alloy (AA 7108) {BenAli2011, BenAli2012}. This choice is motivated by the well documented sensitivity of these alloys to H embrittlement and the possibility to tune the $MgZn_2$ intergranular precipitation and study its impact on cohesion (in the spirit of the CZ modeling above). After H charging, the sample is pulled at various slow strain rates, in wet laboratory air.

At low strain rates, fracture is intergranular brittle. Figure 5 shows the fracture surface obtained at $\dot{\epsilon}_0 = 5\,10^{-7}\,s^{-1}$. Following Gruhl's idea, H, loaded on the side opposite to the notch, diffuses towards the notch's tip in its stress field and induces fracture. We observed that long range stress fields, which have a weak elastic effect on local concentrations, were always extremely efficient in localizing fracture (without notch, cracks initiated where an accidental stress concentrator was found: in the heads, at pits formed during Ni deposit...). The H charging was 48h long. The corresponding penetration depth should be at least of 900 µm which is the distance to the notch's tip from the charging window. This is compatible with the H diffusion coefficient in the absence of traps ($D=10^{-11}$ m^2s^{-1}, for pure Al and under aged 7075 {Scully2012}) which gives $\Lambda \sim 1300$ µm, and the diffusion for the peak aged (T6 7108 was also brittle) with $D=3\ 10^{-12}$ m^2s^{-1} {Scully2012} and $\Lambda \sim 700$ µm, but not with the slow effective diffusion of 10^{-14} m^2s^{-1} (40 µm). Note that, under these H charging conditions, embrittlement is very strain rate dependent. In particular, fracture is ductile beyond $\dot{\epsilon}_0 = 5\,10^{-4}\,s^{-1}$, meaning that equilibrium segregation, which was reached during the 48h of the H pre-charging, alone is not enough to explain the loss of cohesion of the interfaces. We will come back on this point in the atomistic section where we investigate the influence of H on the ideal work of fracture.

Up to now, we have not had the opportunity to apply this method to AlMg alloys, but it would be interesting because the Ni layer allows for an efficient H charging, independent of the emergence of precipitates on the surface, which would enable studying the sensitivity of GBs to H at various β coverages, such as characterized in {Birbilis}, and especially in the absence of β. This is a critical issue if the fracture of the α ligaments in between IG precipitates dictates cohesion. On the other hand, H uptake coupled to intense localized dissolution (as expected by β dissolution at the crack tip) comes with vacancies {Hebert} and might result in a different damage.

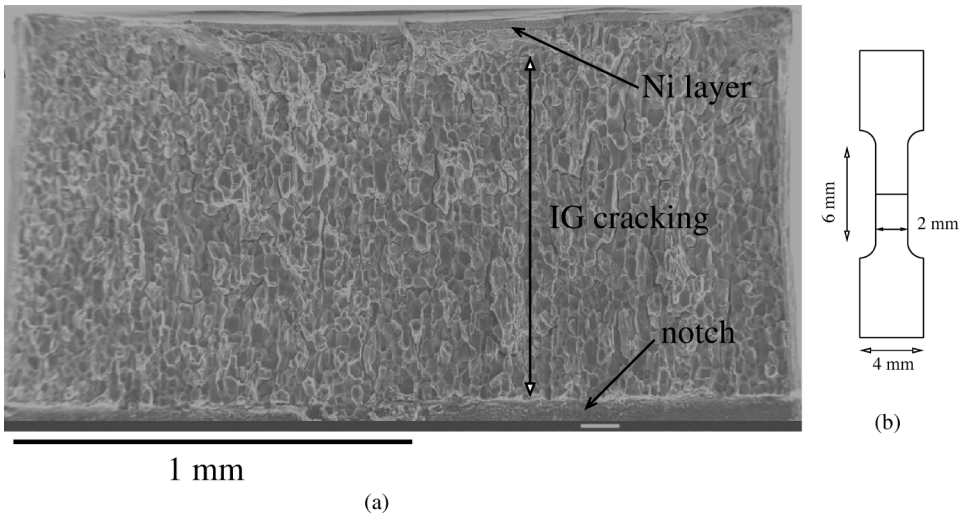

Figure 5:

(a) Intergranular fracture obtained in wet laboratory air by internal hydrogen at a slow strain rate of $5\ 10^{-7}s^{-1}$ on under-aged (T4) AA-7108 (Al-Zn-Mg) {BenAli2011, BenAli2012}. (b) Schematic picture of the sample.

Another question can be addressed in relation to these internal H tests: is H diffusion fast enough to follow the crack?

The CZ model, from the previous section (CZ_1), is enriched by coupling mechanics with diffusion equations. The boundary conditions for H are zero flux on all surfaces, including the crack surfaces (no desorption is possible, as if the oxide layer was a perfect barrier). The initial distribution of H is homogeneous (internal H). First, the crack is loaded slightly below K_{Ic} and H is equilibrated. Then the load is increased above K_{Ic}. The amount of loading above the critical load for crack propagation initiation modifies the numerical rate of propagation ($\acute{a}$). It is tuned to impose $\acute{a}$ to values: 10, 15, 50, 150, 750, 1500 and 7500 nm/s. Two diffusion coefficients (10^{-14} m^2s^{-1} and 10^{-12} m^2s^{-1}) are considered. The model aims at determining if, depending on the diffusion coefficients, H diffusion is a rate limiting process for crack propagation. The two D_{eff} represent diffusion in a field of newly created traps (maybe vacancies, in the case of surface dissolution and short cracks) or intrinsic diffusion (H was created far from the crack tip). The case where H is produced by a local dissolution close to the tip and diffuses directly ahead of the crack tip is not considered.

Figure 4 shows the time evolution of the hydrogen distribution during propagation for two crack velocities. Note that the stationary distribution, when it exists, is not similar to the static distribution. It was found that, at low diffusion coefficient, a stationary distribution ceases to exist between 15 and 50 nm/s, while at $D_{eff}=10^{-12}$ m^2s^{-1}, this transition occurs beyond 1500 nm/s (Fig. 4) {BenAli2012}. According to the average velocities reported in Table 2, it is clear that H diffusion is not a rate limiting process (the velocities are three orders of magnitude smaller). In this case, we can wonder what determines the propagation rate and this is the topic of the atomistic fracture simulations.

Mechanical loading		Environment	Temper	$\acute{v}$ (nm s^{-1})
SSRT	$\acute{\varepsilon}_0 = 5\,10^{-7}\,s^{-1}$ in laboratory air	H pre-charged 48h (Ni Layer) in H_2SO_4 at -800 mV/SCE	T4	10
SSRT	$\acute{\varepsilon}_0 = 5\,10^{-7}\,s^{-1}$ in laboratory air	-	T6	10

Table 2:

Averaged velocities $\acute{v}$ obtained by dividing the intergranular crack length by the duration of the fracture test {BenAli2011, BenAli2012}. The sample geometry and the fracture surface are shown on Fig. 5. The material is the AlZnMg alloy 7108.

Atomistic simulations

In this section, some fundamental aspects of the interaction of H with crystalline defects are addressed. It concerns: H interactions with vacancies (equilibrium concentration of clusters of n H with a vacancy (VH_n), the mobility of VH_n and the consequences on vacancy mediated transport of substitutional solutes and H trapping (D_{eff})); H segregation at grain boundaries and the discussion of the ideal cohesion problem; simulations of intergranular fracture and more specifically the influence of nano cavities on fracture.

We have used a variety of techniques to tackle these issues: DFT calculations, empirical interatomic potentials calibrated on DFT, Monte Carlo simulations (equilibrium and kinetic and therefore saddle searches) and Molecular Statics/Dynamics for fracture. A key issue is the way the limitations of these techniques have been, if not overcome, at least taken into consideration: (i) the quality/precision of the energetic model, (ii) the time scale issue. This paper is not the place to give rigorous, technical, arguments. For that, the reader should refer to specific papers mentioned as references. Instead, only key equations are given and the results, discussions or extrapolations (for example from Ni-H to Al-H) are only qualitative.

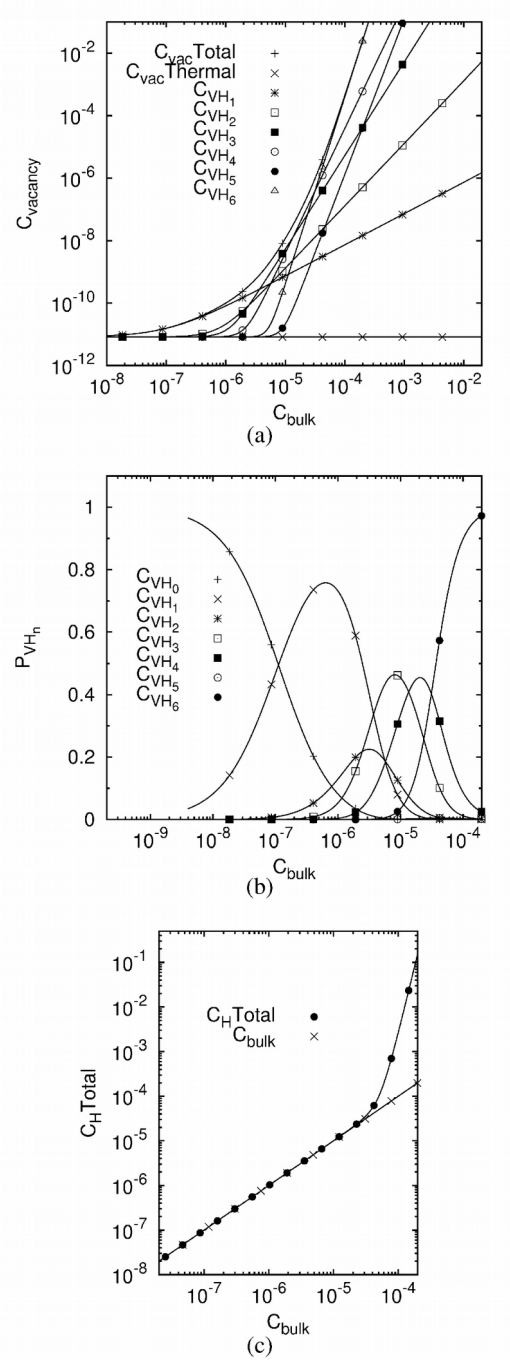

Figure 6:

(a) VH_n concentration (C_{VHn}), at T=300 K, as a function of bulk H concentration (C_{bulk}) in Al; (b) the same data but divided by the total vacancy concentration gives the equilibrium distribution of VH_n (P_{VHn}); (c) the total H concentration (H on bulk interstitial sites plus H trapped in vacancies), from Eq. 2-4 and ab initio data from {Ismer}. C_{VH0} $C_{Vthermal}$ and C_V represent the same thing: the concentration of vacancies free of any H solute.

Throughout the paper, since a concentration is the probability of a site to be occupied by a certain species, all concentrations are atomic concentrations, not weight concentrations (H bulk concentration is the probability a tetrahedral site, in a perfect lattice, is occupied; a vacancy or VH_n concentration is the probability a substitutional site (fcc) is occupied by a vacancy or by a vacancy containing n H).

Vacancies and hydrogen

Fukai {Fukai2001, Fukai1998} has shown that if the conditions are such that vacancy equilibration can occur at experimental time scale, H in interstitial position in the perfect crystal is not the preferential state. Instead, the system increases its stable vacancy concentration to trap most of H. Up to 25% of these clusters were created in Ni at high temperature and high H pressure {Fukai2001}. It has been proposed that such ``superabundant" vacancies can play a role in H damage of metallic alloys {Nagumo2004, Nagumo2014, Tateyama2003, Momida2013}. Theoretically, the energetics of the vacancy-H interaction are known qualitatively for a long time. Norkov {Norskov}, using the Effective Medium Theory, has shown that H in a vacancy occupies positions intermediate between the regular interstitial site and the center of the vacancy. The electronic density there is too low to provide the optimal environment for H which therefore binds to the side of the vacancy. The result is that multiple H can occupy the vacancy. Modern DFT calculations have revisited the problem in Fe {Tateyama2003}, Al {Wolverton, Ismer}, Ni {Tanguy2014} and many other systems {Nazarov}. More quantitative values for segregation and cluster formation energies are now available.

From the DFT calculation of key energetic quantities, simple mean field equation give the equilibrium distribution of VH_n clusters and their concentrations {Ismer, Tanguy2014, Nazarov}, in the dilute limit:

$$\frac{c_{bulk}}{1-c_{bulk}} = e^{-\mu^{¿}/k_B T} \quad (2)$$

$$C_V = e^{-E_f/k_B T} \quad (3)$$

$$C_{VH_k} = n_{VH_k} e^{-\left(E_f + \sum_{i=1}^{k}\left(\Delta E^{i}_{seg} + \sum_{j}\frac{\epsilon_{ij}}{2}\right) + k\mu^{¿}\right)/k_B T} \quad (4)$$

where μ* is a chemical potential which gives the bulk equilibrium H concentration (Eq. 2), as a function of temperature, i.e. the concentration on regular lattice sites, in equilibrium with the VH_k. The free vacancy VH_0 concentration is obtained by Eq. 3, with E_f, the vacancy formation energy. n_{VHk} is the number of equivalent variants for a configuration of *k* H in a vacancy ($n_{VH_k} = 8!/k!(8-k)!$ {Ismer}) and $\left(¿¿ seg^{i} + \sum_{j}^{k} \epsilon_{ij}/2\right)$ $E_f + \sum_{i=1}^{k} ¿$.

is the formation energy of a VH_k configuration that is written as the sum of E_f with *k* times the segregation energy of an isolated H plus repulsive, short range, interactions in between H atoms (ϵ_{ij}) in the vacancy {Tanguy2014}. The solution of these equations are shown on Fig. 6, for T=300 K. The parameters are E_f=0.66 eV {NeugebauerAl} and the cluster formation energy for VH_k is approximated by E_f + k E_{trap} where E_{trap} is the average segregation energy given by Ismer

(table IV in {Ismer}). We don't have access to the details of the various configurations of VH_k, i.e. no way to evaluate the ε_{ij} from Ismer's published data. The results are therefore only qualitative (the C_{bulk} range of stability of the VH_k should be reasonable, but not the proportion P_{VHk} of the different clusters because it is a sensitive data, for example if some non trivial configurations are missing {Tanguy2014}). Figure 6a shows the large enhancement of the vacancy concentration. The bulk H concentration does not go beyond C_{bulk}=200 ppm because the vacancy concentration goes beyond 10% at that concentration and the equations are no longer valid. Nevertheless they only describe equilibrium and if the vacancy production is slow in comparison to H uptake it might be possible, experimentally, to go beyond this value without damaging the crystal. The distribution of VH_n (Fig. 6b), which is the same data as Fig. 6a but simply divided by the total concentration of vacancies, show that the proportion of clusters with less than 2 H atoms remains important up to C_{bulk}=10 ppm (C_{bulk} is always the concentration in the lattice, also called “mobile” H). This has consequences on the cluster mobility, as discussed below.

Taking into account the effect of a solute on VH_n concentrations can be done, in the case of dilute random solid solution, by subtracting the solute-vacancy binding to the formation energy of the vacancy. As E_f appears in a multiplicative factor of all concentrations (Eq. 3 and 4), its modification only involves a vertical translation of the curves in Fig. 6a for the concentration of VH_n in first neighbor of a solute (for the total vacancy concentration a mixing with the concentration on sites with pure Al neighboring has to be made). The influence of a single Mg solute on E_f is small: +0.02 eV according to {Wolverton2007}, i.e. weakling repulsive, in contrast with early quenching experiments (see discussion in {Wolverton2007}).

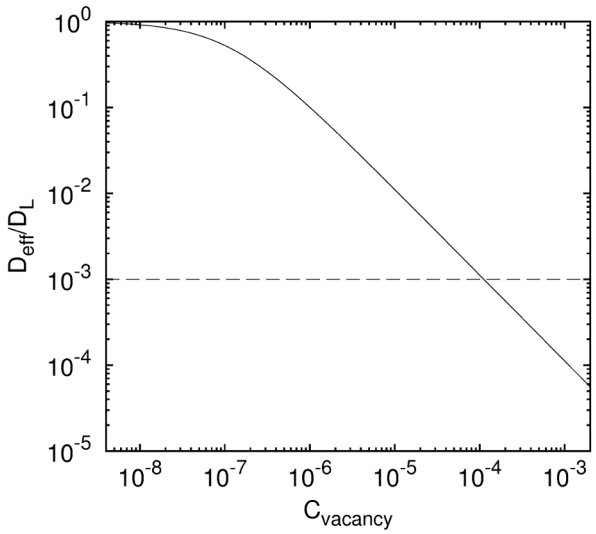

Figure 7:

Variation of the ratio of the effective H diffusion coefficient (D_{eff}) with the lattice diffusion coefficient (D_L) as a function of the vacancy concentration, according to Oriani's formula with a segregation energy on T_1 sites of -0.36 eV (T_1 is the tetrahedral site in first neighbor position of the vacancy).

We can try to extrapolate to Al-H what was found on the Ni-H system {Wang2015}. H in the vacancy has a repulsive interaction with the metal atom which exchanges with the vacancy (Al*). This repulsion increases with a decreasing distance between H and Al*. Therefore, depending on the position of the H atoms in the vacancy with respect to the jump path, the trapped H will more or less increase the activation barrier for the exchange between Al* and the vacancy (E_a). The positions of the 8 tetrahedral sites which can host the H atoms in the vacancy (T_1 sites, i.e. the tetrahedral sites in first neighbor of the lattice site hosting the vacancy {Wang2015}), are such that it is possible to pack H atoms far from the jump path. At least the two most remote T_1 sites should have a minor influence on E_a. We can therefore anticipate that the low E_a (0.57 eV {Ismer}) will not

be too much increased in the case of VH_1 and VH_2 and therefore that vacancies remain mobile at least up to 10 ppm bulk H concentration (the concentration upon which the proportion of such clusters becomes vanishingly small). The corresponding equilibrium concentration of vacancies is about 10^{-8}. The influence of VH_n on the transport of substitutional solutes is discussed further in {Wang2015}.

The impact of vacancies on H mobility can be estimated by calculating the effective diffusion coefficient by Oriani's formula {Oriani, WangActa2015}, in the limit of low H concentrations:

$$D_{eff} = D_L \left(1 + 8\, C_{Vac}\, e^{-\Delta E_{seg}^{T_1}/k_B T}\right)^{-1} \quad (5)$$

where D_L is the lattice diffusion coefficient and $\Delta E_{seg}^{T_1}$ is the segregation energy on the tetrahedral sites inside the vacancy ($\Delta E_{seq}^{T_1} = -0.36$ eV {Ismer}). ΔE_{seg} is the difference in energy of a configuration where H is in the defect and a reference configuration where H is on a bulk site (tetrahedral). It is the opposite of the binding energy (i.e. negative in the case where segregation is favorable). Note that the influence of the different paths to escape the vacancy and the influence of the low diffusion barriers among the different interstitial sites inside the vacancy were studied in {WangActa2015} and were shown to give only second order corrections to Eq. 5. A decrease by three orders of magnitude, such as the one observed in permeation experiments in Al and Al5%Mg in between the second and first H uptake {Scully2012, Scully2013}, would require a very high vacancy concentration, of the order of 10^{-4} (Fig. 7). If created by the H flux, such concentration would correspond to $C_{bulk}=10^{-4}$ and a total H concentration of the order of 1000 ppm (Fig. 6a and c). The clusters will essentially be VH_6 (Fig. 6b) and therefore immobile. In this scenario, the vacancies cannot come from the surface, as mentioned in {Scully2013}. Assuming grain boundaries can produce trap sites at a density of 4 vacancies per a_0^2, where a_0 is the lattice parameter, a grain size of 25 µm would provide $0.5\ 10^{-4}$ such trap sites. The order of magnitude of this effect makes GBs a possible source of the low diffusivity during the first H uptake.

On the contrary, equilibrium bulk VH_n could explain the difference between the measured value for bulk diffusion and the theoretical one. Indeed, a slow down by a factor 10 of H diffusion can be obtained by a concentration of vacancies of 1 ppm, which corresponds to VH_n in equilibrium with $3\ 10^{-5}$ H in the bulk. The proportion of VH_2 is not negligible in these conditions and we can expect the vacancies to be mobile (i.e. they could be generated at GBs and diffuse in the grains to equilibrate the system). This slowdown could explain the discrepancy between the theoretical value for the diffusion coefficient (E_a=0.17 eV and a pre-factor of k_BT/h gives $6\ 10^{-11}$ m²/s) and the measured value (10^{-12} m²/s {Scully2013, Scully2012}).

Intergranular hydrogen segregation

The equilibrium segregation of H to the Σ5{210}[100] {Yamaguchi} and Σ9{221}[110] {Shen} symmetrical tilt grain boundaries was modeled by a combination of DFT calculations and segregation isotherms in a similar way to the vacancy case described above. In the Σ9, the deepest trap has the same energy as the T_1 site of the vacancy: the segregation energy, per H atom, is -0.36 eV. Other sites are favorable with ΔE_{seg} values close to -0.28 eV. Segregation is apparently weaker in the Σ5 with a lowest value of -0.25 eV {Yamaguchi}. No driving forces for the formation of a hydride seed were found {Shen}: H-H interactions are repulsive in between the most favorable sites. The mean field equations predict that such sites become gradually filled, at T=300 K, in between 1 ppm and 10^{-3} H concentration in the bulk. An important role is played by the repulsive H-

H interactions since, once the deepest trap is filled, it repels H from the neighboring sites and therefore shifts their occupancies to higher bulk concentrations (by a factor 10).

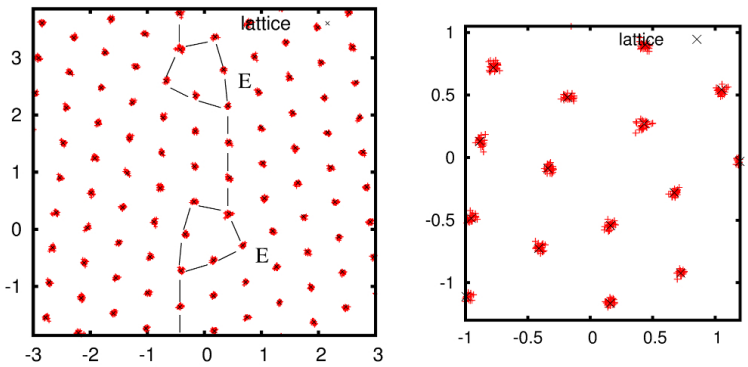

Figure 8:

The CSL unit cell of the Σ33{554}[110] symmetrical tilt grain boundary, composed of E structural units (left) and twin units (right). Unit distance is a_0, the lattice parameter of Al (0.4 nm).

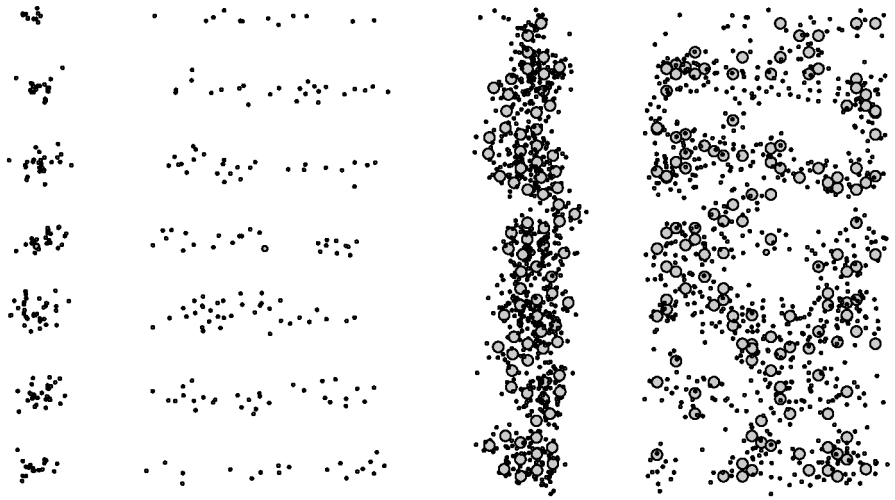

Figure 9:

Segregation of H along the Σ33 GB (Fig. 8). Three CSL units are included in the box, i.e. 6 E units are present. (a) is a view edge on showing a segregation along the tilt axis in the core of the E structural units, (b) is a side view, showing the ladder structure of the E unit cells (analogous to the dislocation lines of an edge dislocation wall). (c) and (d) are the same views with vacancies. The bulk H concentration is 30 ppm and the temperature T=400 K. Only H atoms and vacancies are shown.

The issue of the precision of the calculation can be addressed now. The precision on the segregation energies is estimated to be 40 meV {Shen}, in particular due to the relatively small size of the system containing the GB. At low temperatures, for example 300 K, such error can lead to shifts in the segregation energies by an order of magnitude, i.e. we cannot say if the most favorable site is saturated at 10^{-5} or 10^{-4} bulk H concentrations. The same kind of limitation applies for the vacancy case. At higher temperatures, like the one we considered in Ni {Tanguy2014}, the impact is less important (a factor 5 at 600 K for vacancies in Ni). It does not mean that DFT is not reliable, but that local concentrations at low temperatures are quantities sensitive to the precision on the

segregation energies.

An interesting phenomenon was observed in the Σ9. Two metastable structures were found. The segregation energies were found to be more favorable in the case of the GB with a slightly higher energy. This enhanced capacity to trap hydrogen is related to the capacity of this GB to distort and propose more favorable local environments to H.

The influence of segregated H on the ideal cohesion was investigated with the objective to find critical bulk concentrations that trigger brittleness {Yamaguchi, Shen}. The authors reach opposite conclusions. In brief, the influence of segregated H, in the absence of any H diffusion during fracture, on the work of separation is the difference between the segregation energy to the GB and the one to the surface (multiplied by a term which contains the density of trap sites and their occupancy). In one case {Yamaguchi}, the segregation to the GB is weak (-0.25 eV) and the segregation to the surface is surprisingly strong (-0.7 eV), giving a large driving force for decohesion. In the other case {Shen}, it is the opposite: both values are similar which gives almost no impact of the deep traps and finally a loss of cohesion is possible, but only at high C_{bulk} (beyond 1000 ppm) where weaker traps are populated. This last study is coherent with the early theory of H in metals {Norskov} which shows that deep traps (vacancies, deep GB traps and surfaces) provide the optimal electronic density for H and therefore the segregation energy to these different defects is similar, giving only weak thermodynamic driving force for decohesion. Recent ab initio calculations in other systems show indeed a weak effect in Fe {Momida} and in Ni {ShenS5}. Furthermore, this view is coherent with the experimental observation that GB fracture by internal H is deformation rate dependent (ductile at high velocity).

The failure of the approach combining DFT and mean field equations in the search for a realistic decohesion process motivates the exploration of other paths, more complex and more physical than a separation of the interface without reorganization of the interface. We want to explore the capacity of the GBs to change their structure to accommodate H, as already mentioned above. This time, Monte Carlo simulations which combine atomic displacements, H exchanges and, in the Grand Canonical ensemble, insertion and deletion of metal particles are used {Tanguy2005,Vamvakopoulos}. These simulations, like Molecular Dynamics, rely on continuous interatomic potentials which are, in general, less reliable than DFT (they are acceptable for Al) but are much lighter computationally. Therefore they allow for more intensive exploration of physical processes (many configurations can be explored including these rare configurations which give the saddle energies for thermally activated processes). For the Al-H system, we have updated a potential {Shen} which originally relied on Effective Medium Theory and not fully properly interpreted experimental data {Tanguy2003}. The potential now reproduces the segregation to the vacancy (both the segregation energy value and the off center T_1 position), the segregation to the {111} surface (for fracture), the bulk diffusion barrier (but not the preferential path: the direct jump from a tetrahedral site to another one is slightly preferred to the tetra-octa path). In spite of this update, the test against DFT for the segregation energies on the Σ9 GB shows that this potential underestimates segregation {Shen}, by an amount larger than the precision of the DFT segregation energies. Therefore the bulk concentrations in the simulations have to be increased to compensate. Simulations were conducted on the Σ33{554}[110] symmetrical GB both in $N_{Al}N_HVT$ and in $\mu_{Al}N_HVT$ ensembles. The Σ33 has the same E units (Fig. 8) as the Σ9, which guaranties that the reliability of the potential is under control. The comparison between the two situations (without and with vacancies) is shown on Fig. 9. Without vacancies, H segregates to the core structure of the E units, which gives a ladder structure analogous to segregation on a wall of edge dislocations. When insertion and deletion of Al atoms is possible, the system is largely enriched with VH_n clusters and

the ladder structure is less clear. There seems to be a large driving force for creating VH_n at GBs, which is not a surprise since this trend already exists in the bulk and that vacancy formation energies are lower at GBs. Note, on Fig. 9, that the temperature of 400K was used for a better convergence of the simulation (better sampling of H and vacancy position). More vacancies are expected at 300K.

There are few experimental observations of cavities in Al {Hebert}. More evidences where obtained by Arioka in steels, in creep conditions, where enhanced intergranular fracture by an enhanced intergranular void growth due to H was observed {Arioka2013, Arioka2014}.

The question is now to evaluate the impact of large quantities of vacancies on the cohesion of grain boundaries.

Fracture simulations

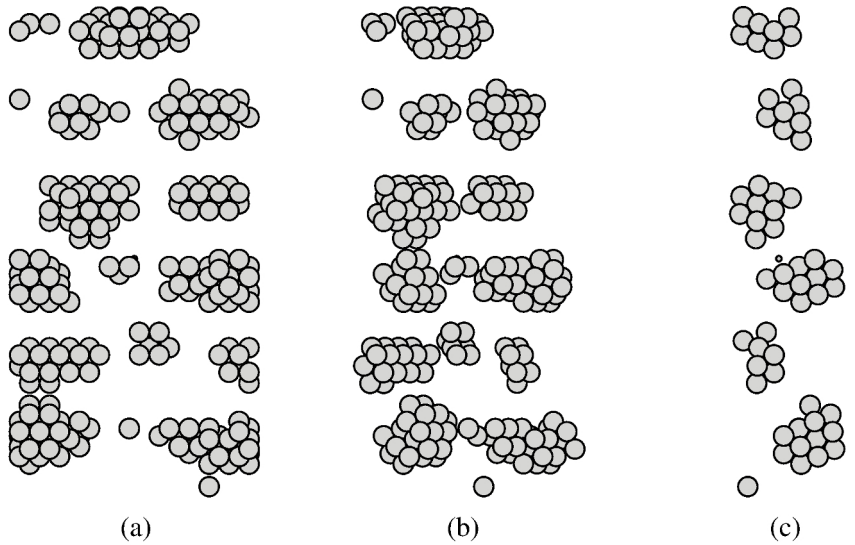

Figure 10:

Nanoscale intergranular cavities (only vacancies are shown) formed under traction (4% strain) in the Σ33 GB of Fig. 8. (a) is a front view (the tilt axis of the GB is horizontal), (b) is tilted and (c) is a side view (tilt axis perpendicular to the figure). There are 6 E units on the picture and periodic boundary conditions are applied.

As a first step, H is dropped out of the simulations but very large vacancy concentrations, reminiscent of the VH_n, are considered. Monte Carlo (MC) simulations were performed at increasing initial strain imposed perpendicular to the interface until vacancies cluster and form nano scale bubbles (Fig. 10). A large box is built by replicating the MC box. An internal intergranular crack is created by removing a few layers. The mechanical properties of the interface are studied by Molecular Statics. The far ends of the sample are rigid and used as mechanical grips. A displacement, perpendicular to the interface, is quasi statically applied. The system is relaxed by Quenched Molecular Dynamics in between load increments. The crack tips are inspected. Two kinds of behaviors are met: if the orientation of the glide planes is favorable, dislocations are emitted; or if glide is difficult or if the GB is weakened by the nanocavities, crack propagation occurs. If emission occurs at a load lower than the one necessary for crack propagation, the crack is said to be intrinsically ductile, by reference to the Rice and Thomson model {Rice1974, Zhou, Thomson,Tanguy2007}.

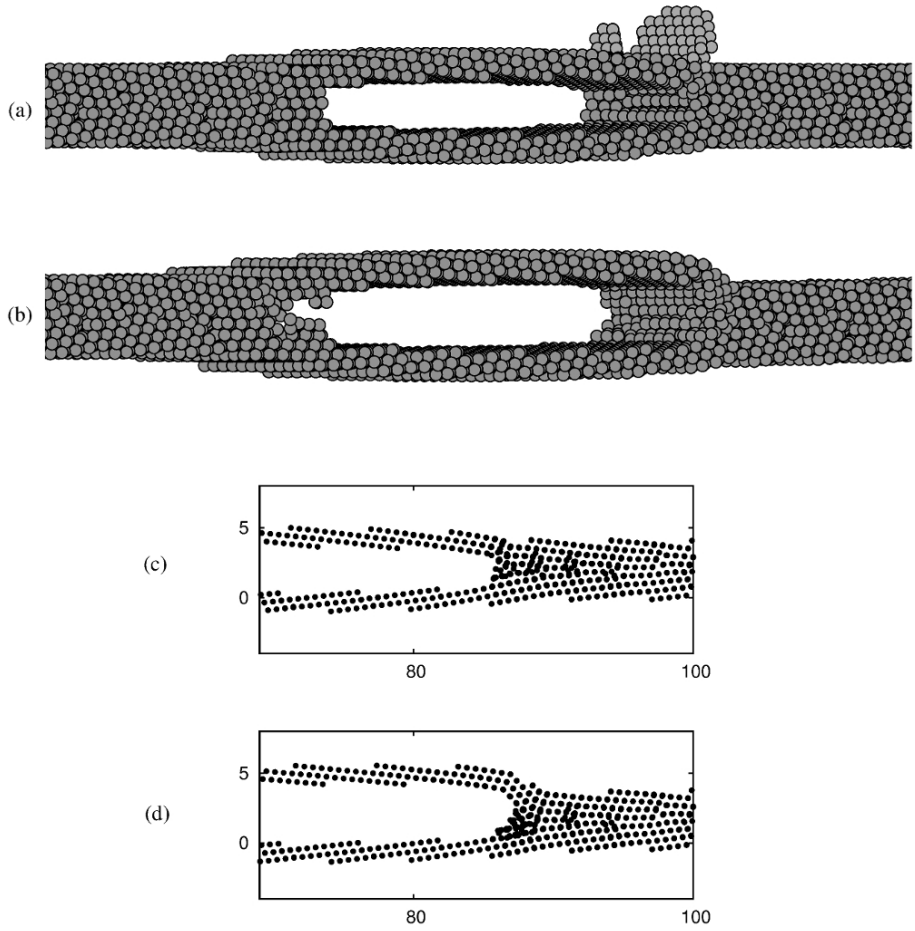

Figure 11:

Dislocation emission from the crack tip: (a) emission of the first half loops (Shockley) and (b) subsequent twinning. Only atoms in a narrow band around the GB are represented. (c) and (d) are corresponding side views which illustrate crack blunting.

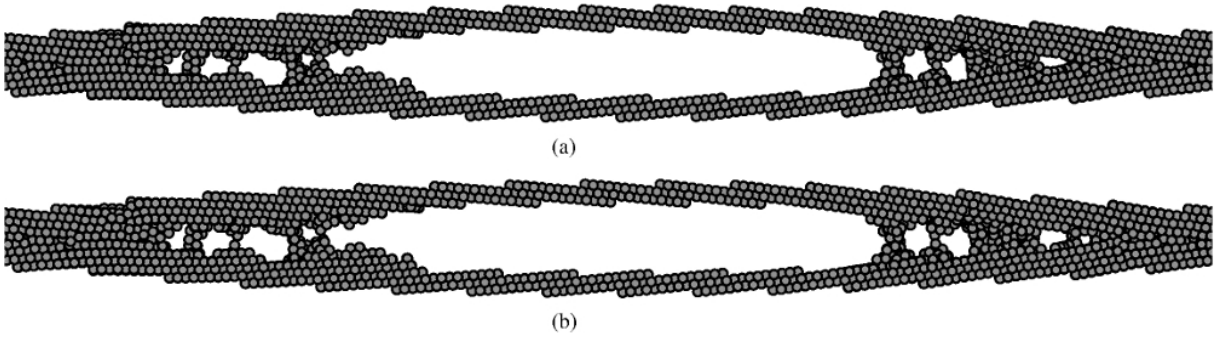

Figure 12:

Side views of a brittle crack during propagation. The labels are coherent with Fig. 13.

In the case of the case of the Σ33 studied here, both crack tips are not equivalent: one is brittle and the other one is ductile. The reason is the geometry of the glide planes with respect to the crack orientation {Cleri}. At the ductile tip, a {111} glide plane intercepts the tip and edge Shockley partials are easily emitted (Fig. 11). The crack tip blunts and the stress concentration decreases. On

the other side, brittle crack propagation can occur. In order to limit dislocation emission, that can have spurious effects on the load necessary for crack propagation on the brittle side, a constraint is implemented in the equations of motion {Tanguy2007} which block the shear localization at the origin of the emission of dislocations. With such setup, brittle cracking can be studied on both sides (Fig. 12). The impact of the size and density of nano scale cavities, such as those shown on Fig. 10, on the critical loads for propagation was studied {Tanguy2015}. It was found that a large density of such clusters have to be present along the GB in order to observe cracking at the expense of dislocation emission. A critical size of 5 vacancies is necessary and a minimum density of the order of one cluster every 8 a_0 along the tilt axis seems to be necessary (i.e. each E unit has a void and the spacing, along the tilt direction, is 8 a_0).

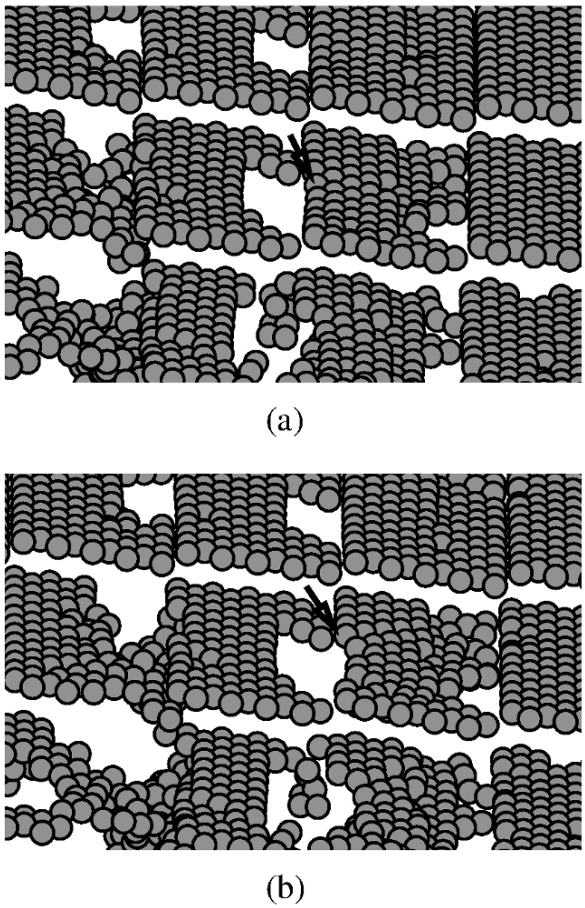

Figure 13:

A zoom on the key mechanism for void growth at zero K. Local glide in between nanocavities: (a) before glide, (b) after glide. The glide zone is marked by arrows.

A close look at the propagation mechanisms reveals that the key event, which triggers void growth, is a local glide in between the nano voids (Fig. 13). No other type of events was detected. It should be stressed here that the temperature is close to 0 in these simulations. As a consequence, only events which activation barrier can be decreased to 0, by concentrating the stresses in the process zone at the crack tip (and in between the cavities), can occur. We are now in the process of studying other types of thermally activated events that would occur, together with such local glides, at finite temperature and long timescales.

Finally, we can attempt to link this study, i.e. the SaV part and the nano-cavity part, with the mechanisms involved in the SCC of Al5%Mg and other fracture mechanisms {Crane2012}. If β

dissolution is the source of H at the crack tip, it is possible that H uptake is coupled with vacancy injection {Hebert}. If H concentration is low enough or the “far from equilibrium” vacancy concentration is large enough not to have saturated vacancies, these remain mobile (although they will move slower than in the absence of H). Therefore, they could segregate to GBs and/or aggregate to form cavities. Furthermore, our study of the impact of nano-scale cavities (although limited to a specific GB) seems to indicate that a high coverage by small cavities is necessary to obtain decohesion. This is related to the formation of a “long” process zone, with a smooth opening profile, which switches off crack tip dislocation emission (and blunting) {Tanguy2015}. This is not in favor of an aggregation of vacancies into large voids but of a homogeneous distribution of VH_n along GBs or a fine dispersion of small cavities. Another aspect is stress concentration ahead of a blunted crack tip (blunted by corrosion during SCC) which transports damage ahead of the tip. It has a signature at the macroscopic scale, for example in the case of the formation of cavities and cracks ahead of round notches in creep conditions {Arioka}. In the case of Al5%Mg, it is tempting to transpose this idea to the nanoscale, with stress concentrations in between β precipitates (Fig. 5 in {BenAli2013}), or at the tip of the precipitates. This would give a length scale χ_{crit} necessary to intermittent cracking models such as the one in {Crane2012}. The problem of the fracture criterion at the position of maximum stress remains. Our position, based on our ab initio calculations {Shen, ShenS5} and Monte Carlo simulations with an empirical potential (Fig. 9 a, b), is that equilibrium H segregation alone does not decrease “cohesion” enough. This comes from the similarity between GB and surface segregation energies which creates only a weak thermodynamic driving force for fracture. The stress effect can be incorporated in the exponential giving the local H concentration in the GB, but the numerical values show that this is a second order correction to the GB segregation energy, even in the range of 1 GPa. Nevertheless, local stress is an ingredient that should be taken into account, together with the local H concentration, in the search for a physical fracture criterion, as we have started to do by looking for thermally activated processes in the PZ of brittle intergranular cracks (i.e. at positions of very high stresses).

Conclusions and perspectives

This paper covers: SCC and H embrittlement experiments on pure; β-free Al5%Mg, the investigation of the fracture of GBs at the surface, at the scale of the grain, in aged and annealed 5083; a continuum mechanics based model of the cohesion of an α/β composite GB and finally some more general considerations concerning intergranular fracture (including experiments on AlZnMg alloys in the case of internal H) and some results from atomistics.

The conclusions are:

(i)

β free grain boundaries can be H embrittled, at least when the material is cold worked, which supports the idea that localized dissolution of β could generate H that would embrittle the α ligament. At free corrosion potential, average crack propagation velocities of the order of 10 nm/s are reported. The comparison between static (with decreasing creep deformation rates) and cyclic (traction-traction) loading suggests a role of dynamic plastic deformation (in preference to a role of the macroscopic stress level) at the crack tip during intergranular SCC.

(ii)

The study of intergranular fracture, at the surface, after H uptake from an electrolyte, shows that: β precipitation is necessary to observe fracture (maybe only to allow H absorption in the material). Fracture occurs, in the annealed state, in between grains which deform less than their neighbors, but embedded in a group of grains which deform preferentially (a macroscopic slip band). This suggests a “grain scale” fracture criterion which is the combination of a local stress level on a facet perpendicular to the traction axis (decohesion), in between two “hard” grains which deform

relatively less than their nearest neighbors.

(iii)

Using cohesive zone models, implemented in finite elements, it is shown that a brittle β ligament will have a weak effect on the overall GB cohesion of a composite GB. Therefore, the modeling efforts should be oriented towards the cohesion of precipitate free GBs.

At that point the paper stops dealing with SCC of AlMg and discusses general issues concerning H embrittlement: the mobility of vacancy-hydrogen clusters and their possible impact on cohesion.

(iv)

The interaction of H with vacancies (in the context of SCC, these are produces by dissolution) in Al is discussed. In particular, recent results obtained on the VH_n mobility in the Ni-H system are extrapolated to Al. A low bulk hydrogen concentration is necessary to maintain a low enough occupation of the vacancies in order to keep them mobile. This concentration is estimated to be about 10 ppm (concentration on the lattice). The mobility of VH_n, which is not compatible with high H concentrations, is an aspect that is worth being taken into account when considering the implication of vacancies in H damage.

(v)

The impact of equilibrium H segregation (i.e. the H which is present in the GB in the absence of any crack inducing dynamical events that would stimulate a time dependent loss of cohesion) on the work of separation seems to be weak i.e. to require large H concentrations (1000 ppm in the lattice and beyond). Therefore, more complex situations are studied by Monte Carlo simulations where equilibration of intergranular vacancies and structure modifications are allowed. Large concentrations of vacancies are found stable at GBs. Their impact, in the form of nano scale cavities, on GB cohesion is studied by Molecular Statics. A critical cavity size/density is found which favors brittle cracking at the expense of dislocation emission from the tip. The mechanisms responsible for cavity growth, at low temperature, are local glide events in between cavities which trigger lattice instability (self interstitials, local cleavage) and favor void coalescence.

Perspectives, on the experimental side, are to use a well controlled H uptake procedure (the Gruhl's hollow tube test that we used on AlZnMg to study the coupling between internal H diffusion and crack dynamics) and follow crack propagation at small scales. Ideally, temperature and H content should be varied and data concerning local crack propagation velocities collected. On the simulation side, the effort should be continued along the line exposed here (role of temperature on the atomistic events occurring in the fracture process zone) with the objective to propose a cohesion model which is time dependent and function of temperature, stress and hydrogen content.

Acknowledgments

This work was supported by Région Rhône Alpes and the french national science fundation (Agence Nationale de la Recherche) under projects ANR-06-BLAN60231 and ANR-10-BLAN19424.

Bibliography

[1] **{Holroyd2011}** N. J. H. Holroyd, G. M. Scamans, Crack propagation during sustained-load cracking of al-zn-mg-cu aluminum alloys exposed to moist air or distilled water, Metallurgical and Materials Transactions A 42A (2011) 3979–3998.
[2] **{Holroyd2013}** N. J. H. Holroyd, G. M. Scamans, Stress corrosion cracking in Al-Zn-Mg-Cu aluminum alloys in saline environments, Metallurgical and Materials Transactions A 44A (2013) 1230–1253.
[3] **{Gangloff}** R. P. Gangloff, Hydrogen assisted cracking of high strength alloys, in: I. Milne, R. O. Ritchie, B. Karihaloo (Eds.), Comprehensive structural integrity, volume 6, Elsevier Science New York, NY, 2003, p. 31.
[4] **{Scully2012}** J. R. Scully, J. G. A. Young, S. W. Smith, Gaseous Hydrogen Embrittlement of Materials in Energy Technologies, volume 1, Woodhead, Cambridge, UK, pp. 707–768.
[5] **{Jones2003}** R. H. Jones, The influence of hydrogen on the stress-corrosion cracking of low-strength al-mg alloys, JOM-Journal of the Minerals Metals & Materials Society 55 (2003) 42–46.
[6] **{Goswami}** R. Goswami, R. L. Holtz, Transmission electron microscopic investigations of grain boundary beta phase precipitation in al 5083 aged at 373 K (100 degrees c), Metallurgical and Materials Transactions A 44A (2013) 1279–1289.
[7] **{Scully2013}** J. H. Ai,M. L. C. Lim, J. R. Scully, Effective hydrogen diffusion in aluminum alloy 5083-h131 as a function of orientation and degree of sensitization, Corrosion 69 (2013) 1225–1239.
[8] **{Crane2012}** C. B. Crane, R. P. Gangloff, Dissolution and hydrogen diffusion control of igscc in sensitized al-mg alloys, in: B. P. Somerday, P. Sofronis (Eds.), Hydrogen Effects on Materials, New York, NY: ASME, 2012, pp. 439–449.
[9] **{Tanguy2002}** D. Tanguy, B. Bayle, R. Dif, T. Magnin, Hydrogen effects during IGSCC of pure al-5%mg alloy in nacl media, Corr. Sci. 44 (2002) 1163.
[10] **{Pouillier}** E. Pouillier, A. F. Gourgues, D. Tanguy, E. P. Busso, A study of intergranular fracture in an aluminium alloy due to hydrogen embrittlement, International Journal of Plasticity 34 (2012) 139.
[11] **{Ohnishi1980}** T. Ohnishi, J. Higashi, J. Jpn. Inst. Light Metals 30 (1980) 560.
[12] **{Malis1982}** T. Malis, M. C. Chaturvedi, Grain-boundary segregation in an Al-8 wt% Mg alloy, J. Mater. Sci. 17 (1982) 1479–1486.
[13] **{Holroyd1985}** N. J. H. Holroyd, G. M. Scamans, The role of magnesium during environment-sensitive fracture of aluminium alloys, Scripa metallurgica 19 (1985) 915–916.
[14] **{Young2002}** G. A. Young, J. R. Scully, The effects of test temperature, temper, and alloyed copper on the hydrogen-controlled crack growth rate of an Al-Zn-Mg-(cu) alloy, Met. Trans. A 33A (2002) 1176–1181.
[15] **{BenAli2012}** N. Ben Ali, D. Tanguy, R. Estevez, Hydrogen embrittlement of AlZnMg alloys: Experiments and simulations, in: B. P. Somerday, P. Sofronis (Eds.), Hydrogen Effects on Materials, New York, NY: ASME, 2012, pp. 697–705.
[16] **{BenAli2011}** N. Ben Ali, D. Tanguy, R. Estevez, Effects of microstructure on hydrogen-induced cracking in aluminum alloys, Scripta Mater. 65 (2011) 210–213.
[17] **{Gruhl1984}** W. Gruhl, Stress-corrosion cracking of high-strength aluminium-alloys, Zeitschrift F¨ur Metallkunde 75 (1984) 819–826.
[18] **{BenAli2013}** N. Ben Ali, R. Estevez, D. Tanguy, Heterogeneity of grain boundaries in 5xxx and 7xxx aluminum alloys and its influence on intergranular toughness, Eng. Frac. Mech. 97 (2013) 1–11.
[19] **{Rose1981}** J. H. Rose, J. Ferrante, J. R. Smith, Universal binding energy curves for metals and bimetallic interfaces, Phys. Rev. Lett. 47 (1981) 675.
[20] **{Needleman1994}** X. P. Xu, A. Needleman, Numerical simulations of fast crack growth in brittle solids., J. Mech. Phys. Solids 42 (1994) 1397–1434.
[21] **{Scamans1976}** G. M. Scamans, R. Alani, P. R. Swann, Pre-exposure embrittlement and stress corrosion failure in AlZnMg alloys, Corros. Sci. 16 (1976) 443–459.
[22] **{Ismer}** L. Ismer,M. S. Park, A. Janotti, C. G. Van deWalle, Interactions between hydrogen impurities and vacancies in mg and al: A comparative analysis based on density functional theory, Phys. Rev. B 80 (2009) 184110.
[23] **{Fukai2001}** Y. Fukai, Y. Shizuku, Y. Kurokawa, Superabundant vacancy formation in nih alloys, Journal of Alloys and Compounds 329 (2001) 195–201.
[24] **{Fukai1998}** E. Hayashi, Y. Kurokawa, Y. Fukai, Hydrogen-induced enhancement of interdiffusion in cu-ni diffusion couples, Phys. Rev. Lett. 80 (1998) 5588.
[25] **{Nagumo2004}** M. Nagumo, Hydrogen related failure of steels - a new aspect, Materials Science and Technology 20 (2004) 940.
[26] **{Nagumo2014}** M. Hatano, M. Fujinami, K. Arai, H. Fujii, M. Nagumo, Hydrogen embrittlement of austenitic stainless steels revealed by deformation microstructures and strain-induced creation of vacancies, acta mat. 67 (2014) 342–353.
[27] **{Tateyama2003}** Y. Tateyama, T. Ohno, Stability and clusterization of hydrogenvacancy complexes in -fe: An ab initio study, Phys. Rev. B 67 (2003) 174105.
[28] **{Momida2013}** H. Momida, Y. Asari, Y. Nakamura, Y. Tateyama, T. Ohno, Hydrogen-enhanced vacancy embrittlement of grain boundaries in iron, Phys. Rev. B 88 (2013) 144107.
[29] **{Norskov}** J. K. Norskov, F. Besenbacher, Theory of hydrogen interaction with metals, Journal of the less-common metals 130 (1987) 475–490.

[30] **{Wolverton}** C. Wolverton, V. Ozolin¸ ˇs, M. Asta, Hydrogen in aluminum: First-principles calculations of structure and thermodynamics, Phys. Rev. B 69 (2004) 144109.
[31] **{Tanguy2014}** D. Tanguy, Y. Wang, D. Connétable, Stability of vacancy-hydrogen clusters in nickel from first-principles calculations, acta mat. 78 (2014) 135–143.
[32] **{Nazarov}** R. Nazarov, T. Hickel, J. Neugebauer, Ab initio study of H-vacancy interactions in fcc metals: Implications for the formation of superabundant vacancies, Phys. Rev. B 89 (2014) 144108.
[33] **{Glensk}** A. Glensk, B. Grabowski, T. Hickel, J. Neugebauer, Breakdown of the arrhenius law in describing vacancy formation energies: The importance of local anharmonicity revealed by ab initio thermodynamics, Phys. Rev. X 4 (2014) 011018.
[34] **{Wang2015}** Y. Wang, D. Connétable, D. Tanguy, Hydrogen influence on diffusion in nickel from first-principles calculations, Phys. Rev. B 91 (2015) 094106.
[35] **{Oriani}** R. A. Oriani, Diffusion and trapping of hydrogen in steel, acta metallurgica 18 (1970) 147.
[36] **{WangActa2015}** Y. Wang, D. Connétable, D. Tanguy, Influence of trap connectivity on H diffusion: vacancy trapping, acta mater. 103 (2015) pp. 334-340
[37] **{Yamaguchi}** M. Yamaguchi, K. Ebihara, M. Itakura, T. Kadoyoshi, T. Suzudo, H. Kaburaki, First-principles study on the grain boundary embrittlement of metals by solute segregation: Part ii. metal (fe, al, cu)-hydrogen (h) systems, Metall. Mater. Trans. A 42 (2011) 330.
[38] **{Shen}** X. J. Shen, D. Tanguy, D. Connétable, Atomistic modelling of hydrogen segregation to the _9{221}[110] symmetric tilt grain boundary in al, Philos. Mag. 94 (2014) 2247–2261.

[39] **{Tanguy2005}** D. Tanguy, M. Mareschal, Superabundant vacancies in a metalhydrogen system: Monte carlo simulations, Phys. Rev. B 72 (2005) 174116.
[40] **{Vamvakopoulos}** E. Vamvakopoulos, D. Tanguy, Equilibrium vacancy concentrations in Al-_Σ= 33(554)[110] by grand canonical monte carlo simulations, Phys. Rev. B 79 (2009) 094116.
[41] **{Tanguy2003}** D. Tanguy, T.Magnin, Atomic-scale simulation of intergranular segregation of h in almg: implications for h-induced damage, Philos. Mag. 83 (2003) 3995–4009.
[42] **{Cleri}** F. Cleri, S. R. Phillpot, D. Wolf, Atomistic simulations of integranular fracture in symmetric-tilt grain boundaries, Interface science 7 (1999) 45–55.
[43] **{Tanguy2007}** D. Tanguy, Constrained molecular dynamics for quantifying intrinsic ductility versus brittleness, Phys. Rev. B 76 (2007) 144115.
[44] **{Tanguy2015}** D. Tanguy, Critical intergranular cavity density for a transition from intrinsic ductility to brittleness, in preparation.
{Needleman1987} A. Needleman, Continuum model for void nucleation by decohesion debonding, J. Appl. Mech. 54 (1987) pp. 525-531

{VanDerVen} A. Van der Ven and G. Ceder, The thermodynamics of decohesion, Acta Mater. 52 (2004) pp. 1223-1235

{Birbilis} N. Birbilis, R. Zhang, M. L. C. Lim, Qunatification of Sensitization in AA5083-H131 via Imaging Ga-Embrittled Fracture Surfaces, Corrosion 69 (2013) pp. 396-402

{Hebert} S. Adhikari, L. S. Chumbley, H. Shen, Y. C. Jean, A. C. Geiculescu, A. C. Hillier and K. R. Hebert, Interfacial voids in aluminum created by aqueous dissolution, Electrochimica Acta 55 (2010) pp. 6093-6100

{Wolverton2007} C. Wolverton, Solute-vacancy binding in aluminum, Acta Mater. 55 (2007) 5867-5872

{Norskov} J. K. Norskov and F. Besenbacher, Theory of hydrogen interaction with metals, Journal of Less-common metals 130 (1987) pp. 475-490

{Momida} H. Momida, Y. Asari, Y. Nakamura, Y. Tateyama and T. Ohno, Hydrogen enhanced vacancy embrittlement of grain boundaries in iron, Phys. Rev. B 88 (2013) art. 144107

{ShenS5}. X. J. Shen, D. Connétable and D. Tanguy, H and vacancy segregation at the Σ5(210)[001] GB in Ni: impact on the ideal work of separation (in preparation).

{Arioka2013} K. Arioka, T. Miyamoto, T. Yamada and M. Aoki, Role of cavity formation in crack initiation of cold worked carbon steel in high-temperature water, Corrosion 69 (2013) p. 487

{Arioka2014} K. Arioka, Change in bonding strength at grain boundaries before long-term SCC ignition, Corrosion 71 (2014) p. 403

{Rice1974} J. R. Rice and R. Thomson, Ductile versus brittle behavior of crystals, Philos. Mag. 29 (1974) p. 73

{Zhou} S. J. Zhou, A. E. Carlsson and R. Thomson, Crack blunting effects on dislocation emission from cracks, Phys. Rev. Lett. 72 (1994) 852

{Thomson} S. J. Zhou, A. E. Carlsson and R. Thomson Dislocation nucleation and crack stability: Lattice Green's-function treatment of cracks in a model hexagonal lattice, Phys. Rev. B 47 (1993) 7710

{Osamura} K. Osamura and T. Ogura, Metastable phases in the early stage of precipitation in Al-Mg alloys, Met.

Trans. A 15A (1984) pp. 835-842

{Holroyd2015} S. P. Knight, K. Pohl, N. J. H. Holroyd, N. Birbilis, P. A. Rometsch, B. C. Muddle, R. Goswami and S. P. Lynch, Some effects of alloy composition on stress corrosion cracking in Al-Zn-Mg-Cu alloys, Corrosion Science 98 (2015) pp. 50-62